[Regular Paper]

Numerical Simulation of Oil Dispersions in Vertical Pipe Flow

Mahdi PARVINI, Bahram DABIR*, and Seyed Abolfazl MOHTASHAMI

Dept. of Chemical Engineering, Amirkabir University of Technology, Hafez St., P.O. Box 15875/4413 Tehran, IRAN

(Received October 27, 2008)

Immiscible liquid dispersions are widely used in chemical process, petroleum industries, polymerization, heterogeneous chemical synthesis, etc. In most of these chemical processes, the rate of inter-phase heat and mass transfer is known to strongly affect the overall performance and depends on the interfacial contact area between the phases. This study at CFD simulations of immiscible liquid dispersion has been performed on a vertical pipe. With specific reference to dispersed liquid-liquid flows, it was seen that the two-fluid approach (Eulerian-Eulerian approach) was extensively used for multiphase modeling, especially when detailed predictions are desirable over a range of holdups in exchange for a reasonable amount of computation power. The results of CFD predictions for water as a continuous and kerosene as a dispersed phase have been compared with the experiments of Farrar and Bruun and Al-Deen and Bruun. These simulations have also been done to understand the effect of various significant forces in turbulent liquid dispersions (drag, lift, turbulent dispersion and added mass). Several expressions for these forces were tested in order to choose the best combination. Further, the problem has been simulated using two different turbulence models. It has been found that lift force is more important than turbulent dispersion and added mass. Inter-phase closure guidelines for liquid-liquid bubbly flows were developed based on simulation results that yielded the best agreement with experimental data.

Keywords

Numerical simulation, Computational fluid dynamics, Immiscible dispersion, Vertical pipe flow, Interface force

1. Introduction

In chemical process industries, liquid-liquid dispersions are commonly encountered, for example, in solvent extraction, emulsification, polymerization, heterogeneous chemical synthesis, direct contact heat transfer, homogenization process. For optimal design and efficient operation of equipments handling such dispersions, it is imperative that a qualitative and quantitative understanding of the hydrodynamics to be developed. Also the mass and heat transfer between the dispersed and continuous phases assumes additional importance in the production, processing and transport of products. Experiments can yield significant insight into the factors affecting the interfacial area. However, problems such as limited range of applicability of the empirical correlations so developed, difficulty in extrapolating the inferences to other geometries or even scaled-up versions of the same equipment, and overall cost and time frame limitations have led to more attention being focused on numerical approaches such as computational fluid dynamics (CFD). This is particularly true for multi-fluid flow in complex geometries. The proven success of CFD to accurately predict the hydrodynamics in most single-phase flows cannot be readily translated to the case of multiphase dispersions.

The presence of the dispersed phase invariably introduces additional complexities. Nevertheless, if fundamental multiphase characteristics such as the dispersed phase holdup could be accurately predicted, it would be easier to estimate the contact area and the dynamics of the dispersed phase (size distributions, breakup, coalescence, etc.).

There are several known approaches to model dispersed two-phase flows using CFD. Some of the commonly used ones are the two-fluid (Eulerian-Eulerian), discrete phase (Eulerian-Lagrangian), and interface tracking (volume of fluid) approaches. Amongst the aforementioned approaches, the two-fluid approach is widely used. Although there are several studies in context of turbulent bubbly flows, a large number of these studies are found on gas-liquid systems (Friberg[1]; Thakre and Joshi[2]; Joshi[3]; Sokolichin *et al.*[4]; Deen *et al.*[5]; Dhotre and Joshi[6]). It is well known that concepts and results related to gas-liquid systems cannot be readily applied to liquid-liquid systems owning to small density differences and high viscosity ratios (Jin *et al.*[7]; Brauner[8]; Shi *et al.*[9]; Madhavan, S.[10]). Because the closure requirements for immiscible liquid dispersion

* To whom correspondence should be addressed.
* E-mail: drbdabir@aut.ac.ir

systems has received relatively lesser attention, the present paper, therefore, attempts to fill this void by means of an organized study which clearly distinguishes and quantifies the various significant forces acting on the dispersed phase in immiscible liquid dispersions.

1. 1. Treatment of Inter-phase Forces in Dispersed Multi-fluid Flow

It is well known that in dispersed multiphase flows, inter-phase forces play a significant role in determining the local phase distribution (Jakobsen *et al.*[11]; Friberg[1]; Deen[5]; Joshi[3]; Ranade[12]; Worner[13]; Chen *et al.*[14]; Tabib *et al.*[15]). Some of the typical interface forces encountered in multi-fluid dispersion are gravitational and buoyancy force, drag force, lift force, virtual/added mass force, Basset force, wall lubrication force and turbulent dispersion.

1. 2. Liquid-liquid Dispersion in Vertical Flow

Most of the previous CFD related studies have focused on extraction columns (Rieger[16]; Modes and Bart[17]; Vikhansky and Kraft[18]) or mechanically agitated tanks (Alopaeus *et al.*[19]; Agterof *et al.*[20]). These configurations suffer from the presence of complex hydrodynamics with very large spatial variation in energy dissipation rates and feature a wide range of circulation times. In this paper, the vertical pipe was chosen as the geometry of interest as it featured simple hydrodynamics in addition to an extensive database of accurate experimental results (Farrar and Bruun[21]; Al-Deen and Bruun[22]).

Liquid-liquid pipe flows are encountered in a broad range of operations such as the production, processing and transport of petroleum resources, direct contact heat transfer and various reaction engineering operations. Domgin *et al.*[23] studied the turbulent dispersion of drops in a vertical pipe. They used the Eulerian-Lagrangian approach to simulate the experimental work of Calabrese and Middleman[24] on the turbulent dispersion of drops in a vertical pipe (50.8 mm ID and 9.1 m long). Hamad *et al.*[25] simulated kerosene-water upflows in a vertical pipe (78 mm ID and 1.5 m long) and compared their results with the experimental data of Farrar[26].

1. 3. Multiphase and Turbulence Modeling Approach

Domgin *et al.*[23] used the Eulerian-Lagrangian approach in their work, as one of their objectives was to couple a lagrangian model to commercial CFD code and improve the basic k-ε formalism using algebraic stress relations for non-isotropic turbulent flow. Their lagrangian model did not take into account dispersed fluid rotation, dispersed fluid collisions or turbulence modulation of the carrier (continuous) phase due to the presence of dispersed phase. An alternative approach (called the Reynolds Stress Model or RSM) was also tested where the turbulence in the carrier flow was predicted using second order turbulence model, which would directly compute the fluctuating velocity correlations. However, since the improvements brought by RSM turbulence model did not justify the additional CPU time requirements, it was not used in their final simulations. Also, in their work the value of σ_k, a constant in the transport equation for the continuous phase turbulent kinetic energy was modified from its default value of 1 to 2.3, in order to obtain a numerical profile for the turbulent kinetic energy which was in good agreement with the experimental data of Sabot[27] for turbulent pipe flow. In another investigation, Hamad *et al.*[25] used the two-fluid Eulerian-Eulerian model to predict the dispersed phase volume fraction and phase velocity distribution for kerosene-water up-flows in a vertical pipe. Their preliminary single phase predictions (velocity and turbulence intensity profiles) reported very good agreement with experimental data. In their liquid-liquid CFD simulations, the velocity profiles for both phases were predicted quite accurately. However, they were unable to precisely predict the distribution of the dispersed phase volume fraction, particularly the characteristic near-wall peak. They attributed this discrepancy to uncertainty in the experimental data as well as the insufficient treatment of inter-phase forces. While transport equations for the turbulent kinetic energy and turbulent energy dissipation rate were solved for the continuous phase, there was no mention of how the turbulence in the dispersed phase was accommodated. It was, however, mentioned that their k-ε model did not take into account drop-induced turbulence (*e.g.* similar to the models developed by Lance and Bertodano[28] and Bertodano *et al.*[29] for bubbles).

1. 4. Treatment of Drop Diameter

Calabrese and Middleman[24] had observed in their experiments that the drop diameter did not have a significant influence on the radial dispersion. As a result, they proposed a single curve for the radial drop dispersion irrespective of the drop diameter. Domgin *et al.*[23] used a constant uniform drop diameter in all their simulations which were based on the experimental conditions of Calabrese and Middleman[24]. Interestingly, it was seen from the simulations of Domgin *et al.*[23] that unlike the experimental observations of Calabrese and Middleman[24], the degrees of dispersion for different diameter drops were clearly distinct, particularly for drops more dense than water. In the other study by Hamad *et al.*[25] there was no mention of how the drop diameter was treated in their CFD simulations.

1. 5. Interface Forces

Both Domgin *et al.*[23] and Hamad *et al.*[25] used the standard drag expression for a single rigid sphere throughout their simulation. Hamad *et al.*[25] considered non-drag inter-phase forces to be minor additional forces and consequently did not account for them in their simulations. On the other hand, Domgin *et al.*[23] studied

the effect of virtual mass, pressure effects, and the basset (or history) terms in their simulations. They justified the inclusion of the virtual mass force in their study on the basis of a wide range of density ratios involved in their investigations. Nevertheless, it was seen from their simulations that the basset and pressure terms had a weak influence on the results. It should be noted that Domgin *et al.*[23] also did not consider the effect of lift forces in their simulations.

2. Mathematical Model

While there are several formulations of Eulerian-Eulerian approach, the form of governing equations as proposed by Ishii[30] is most commonly used in fluid-fluid flows. The basis for the governing equations has been discussed in detail by Van Wachem and Almstedt[31]. The two-fluid Eulerian-Eulerian approach is used in the current paper solving the following conservation equations:

2. 1. Conservation of Mass (equation of continuity)

Conservation of mass for any phase (q) is given by the following transport equation:

$$\frac{\partial}{\partial t}(\alpha_q \rho_q) + \nabla.(\alpha_q \rho_q \vec{v}_q) = \left(\sum_{p=1}^{n} \dot{m}_{pq} - \alpha_q \frac{d\rho_q}{dt} \right) \quad (1)$$

The solution of this equation for each phase, considering the condition that the phase volume fractions should sum to unity, allows for the calculation of individual phase volume fractions.

2. 2. Conservation of Momentum

The conservation of momentum for a continuous fluid phase 'q' in a non-accelerating frame of reference is given by:

$$\frac{\partial}{\partial t}(\alpha_q \rho_q \vec{v}_q) + \nabla.(\alpha_q \rho_q \vec{v}_q \vec{v}_q) = -\alpha_q \nabla P + \nabla.\overrightarrow{\tau_q} + \alpha_q \rho_q \vec{g} + \left(F_{drag,q} + F_{Lift,q} + F_{VM,q}\right) + \sum_{p=1}^{n} \left(K_{pq}(\vec{v}_p - \vec{v}_q) + \dot{m}_{pq} \vec{v}_{pq} \right) \quad (2)$$

Where the q-th phase stress tensor, t_q, for laminar flow is given by:

$$\vec{\tau} = \alpha_q \mu_q \left(\nabla \vec{v}_q + \nabla \vec{v}_q{}^T \right) + \alpha_q \left(\lambda_q - \frac{2}{3} \mu_q \right) \nabla v_q \vec{I} \quad (3)$$

Here μ_q and λ_q are the shear and bulk viscosity of phase 'q.' The relative velocity between the continuous and dispersed phase is given by $(\vec{v}_p - \vec{v}_q)$, where '$\vec{I}$' is a unit tensor and 'p' is the pressure shared by all phases. The bulk viscosity is typically ignored in fluid-fluid flows as it assumes importance only in gas-solid flow and flow that feature shock waves, absorption and attenuation of acoustic waves, etc. (Rande[12]).

For steady-state incompressible flow in the absence of mass transfer, external body forces such as the centrifugal forces, and virtual mass effects (which assume significance only when high-frequency fluctuations of the relative velocity are predominant; Drew[32]; Chen *et al.*[14]), the momentum conservation equation simplifies to:

$$\nabla.(\alpha_q \rho_q \vec{v}_q \vec{v}_q) = -\alpha_q \nabla P + \nabla.\overrightarrow{\tau_q} + \alpha_q \rho_q \vec{g} + F_{Lift,q} + \sum_{p=1}^{n} \left(K_{pq}(\vec{v}_p - \vec{v}_q) \right) \quad (4)$$

The forces indicated above represent the inter-phase drag force, lift force, virtual mass force and turbulent dispersion force, respectively. In the present hydrodynamic model all forces have been used. A brief description of each interfacial force component is presented below.

The origin of the drag force is due to the resistance experienced by a body moving in the liquid. Viscous stress creates skin drag and pressure distribution around the moving body creates form drag. The latter mechanism is due to inertia and becomes significant as the dispersed fluid Reynolds number becomes larger. The inter-phase momentum transfer between gas and liquid due to drag force is given by:

$$F_{drag,q} = -\frac{3}{4} \alpha_q \rho_q \frac{C_D}{d_p} |v_p - v_q| (v_p - v_q) \quad (5)$$

Where, C_D is the drag coefficient taking into account the character of the flow around the bubble and d_p is the dispersed fluid diameter, the lift force arises from the net effect of pressure and stress acting on the surface of a bubble. The lift force in terms of the slip velocity and the curl of the liquid phase velocity can be described as:

$$F_{Lift,q} = C_L \alpha_q \rho_q (v_p - v_q) \nabla \times v_q \quad (6)$$

Where, C_L is the lift coefficient; the sign of this force depends on the orientation of slip velocity with respect to the gravity vector.

When a bubble or drop moves in a liquid field with a non-uniform velocity, it accelerates some of the liquid in its neighborhood. Due to the acceleration induced by the bubble or drop motion, the surrounding liquid experiences an extra force, which is due to the motion in a non-inertial frame of reference, called virtual or added mass force. Then the virtual mass force is proportional to relative phase accelerations as follows:

$$F_{VM,q} = -F_{VM,p} = C_{VM} \alpha_q \rho_q \left(\frac{dv_q}{dt} - \frac{dv_p}{dt} \right) \quad (7)$$

This force was neglected in all the previous simulations in accordance with the observations made by Hunt *et al.*[33], Thakre and Joshi[2], Deen *et al.*[5], and Sokolichin *et al.*[4].

The turbulent dispersion force, derived by Lopez de Bertodano[34] is based on the analogy with molecular movement. It approximates a turbulent diffusion of the bubbles by the liquid eddies. It is formulated as:

$$F_{TD} = -C_{TD}\rho_q k \nabla \alpha_q \quad (8)$$

Where, k is the liquid turbulent kinetic energy per unit of mass. C_{TD} is the turbulent dispersion coefficient.

2. 3. Turbulence Equations

The Reynolds-averaged Navier-Stokes (RANS) equations govern the transport of the averaged tow quantities, with the whole range of the scales of turbulence being modeled. Entire hierarchies of closure models are available in FLUENT including Spalart-Allmaras, k-ε and its variants, k-ω and its variants, and the RSM.

Large Eddy Simulation (LES) provides an alternative approach in which large eddies are explicitly computed (resolved) in a time-dependent simulation using the Navier-Stokes equations. This model was not considered in present paper.

2. 3. 1. k-ε Turbulence Model

One of the most prominent turbulence models, the k-ε model, has been implemented in most general purpose CFD codes and is considered the industry standard model.

In this model continuous phase turbulence is usually modeled using transport equations of 'k' and 'ε' which are written in a form similar to those found in single phase flow:

$$\frac{\partial}{\partial t}\left(\alpha_q \rho_q \varphi_q\right) + \nabla.\left(\alpha_q \rho_q \vec{v}_q \varphi_q\right) = \nabla.\left(\alpha_q \frac{\mu_{t,q}}{\sigma_\varphi} \nabla \varphi_q\right) + S_{\varphi q} \quad (9)$$

Where, φ_q can be the turbulent kinetic energy or the turbulent energy dissipation rate of the continuous phase 'q.' The symbols $\mu_{t,q}$ and σ_φ refer to the turbulent viscosity and the turbulent Prandtl number for 'k' and 'ε' of the continuous phase.

The term '$S_{\varphi q}$' in Eq. (9) is the source term for the quantity, φ. This can be further expanded as below:

$$S_{kq} = \alpha_q G_{kq} - \alpha_q \rho_q \varepsilon_q + \alpha_q \rho_q \Pi k_q \quad (10)$$

$$S_{\varepsilon q} = \alpha_q \frac{\varepsilon_q}{k_q}\left[C_{\varepsilon 1} C_{kq} - C_{\varepsilon 2}\rho_q \varepsilon_q\right] + \alpha_q \rho_q \Pi \varepsilon_q \quad (11)$$

Here, C_{kq} represent the turbulent kinetic energy generation due to mean velocity gradients in phase 'q,' and is again calculated in a fashion similar to single-phase flows, where:

$$G_{kq} = -\rho \overline{\acute{v}_i \acute{v}_j} \frac{\partial v_j}{\partial x_i} \quad (12)$$

Extra generation or dissipation of turbulence due to the presence of the dispersed phase (*i.e.* turbulence modulation) is accounted for in the last terms of expressions for S_{kq} and $S_{\varepsilon q}$ respectively (*i.e.* $\alpha_q \rho_q \Pi k_q$ and $\alpha_q \rho_q \Pi \varepsilon_q$). There have been several attempts to develop models in order to represent such extra terms and these were reviewed by Lahey[35] and recently by Peirano and Leckner[36].

The continuous phase turbulent viscosity is calculated using an expression similar to that used in single phase flows:

$$\mu_{t,q} = \rho_q C_\mu \frac{k_q^2}{\varepsilon_q} \quad (13)$$

The standard k-ε turbulence model contains certain empirical constants which are listed in **Table 1**.

Table 1 Standard k-ε Turbulence Model Constants (Madhavan[10])

Model parameter	Default (suggested) value
$C_{\varepsilon 1}$	1.44
$C_{\varepsilon 2}$	1.92
C_m	0.09
s_k	1
s_e	1.3

2. 3. 2. Reynolds Stress Modeling (RSM) Turbulence Model

In flows where the turbulent transport or non-equilibrium effects are important, the eddy-viscosity assumption is no longer valid and results of eddy-viscosity models might be inaccurate. In the RSM model, individual Reynolds stresses are computed *via* a differential transport equation. The exact form of Reynolds stress transport equations is derived by taking moments of exact momentum equation. Thus, the RSM model solves six Reynolds stress transport equations. Along with these, an equation for dissipation rate is also solved. The exact transport equation for the transport of Reynolds stresses is given by:

$$\frac{\partial}{\partial t}\left(\alpha_q \rho_q \overline{\acute{v}_i \acute{v}_j}\right. + \frac{\partial}{\partial x_k}\left(\alpha_q \rho_q v_k \overline{\acute{v}_i \acute{v}_j}\right. = \alpha_q P'_{ij} + \alpha_q \Phi_{ij} + \frac{\partial}{\partial x_k}\left(\alpha_q\left(\mu_q + \frac{2}{3} C_s \rho \frac{k^2}{\varepsilon_q}\right)\frac{\partial \overline{\acute{v}_i \acute{v}_j}}{\partial x_k}\right) - \frac{2}{3}\delta_{ij}\alpha_q \rho_q \varepsilon_q \quad (14)$$

where Φ_{ij} is the pressure-strain correlation, and P', the exact production term, is given by:

$$P' = -\rho_q\left(\overline{\acute{v}_i \acute{v}_j}\left(\nabla v\right)^T + \left(\nabla v\right)\overline{\acute{v}_i \acute{v}_j}\right. \quad (15)$$

As the turbulence dissipation appears in the individual stress equations, an equation for ε is computed with the model transport equation:

$$\frac{\partial}{\partial t}\left(\alpha_q \rho_q \varepsilon_q\right. + \frac{\partial}{\partial x_i}\left(\alpha_q \rho_q v_i \varepsilon_q\right. = \frac{\partial}{\partial x_i}\left(\alpha_q\left(\mu_q + \frac{\mu_{t,q}}{\sigma_\varepsilon}\right)\frac{\partial \varepsilon_q}{\partial x_j}\right) + \alpha_q C_{\varepsilon 1}\rho_q\left(\overline{\acute{v}_i \acute{v}_k}\frac{\partial v_i}{\partial x_k}\right)\frac{\varepsilon_q}{k} - C_{\varepsilon 2}\rho_q \alpha_q \frac{\varepsilon_q^2}{k} \quad (16)$$

k is calculated from the solved values of normal stress using the Reynolds stress transport equation, as

$$k = \frac{1}{2}\left(\sum_{i=1,2,3} \acute{v}_i \acute{v}_j \right. \quad (17)$$

Turbulence in the dispersed phase may be physically understood as dispersed fluid velocity fluctuation caused by inter-dispersed fluid collisions and inter-

actions of the dispersed fluids with the turbulent continuous phase (Balzer *et al.*[37]; Simonin[38]; Enwald *et al.*[39]). However, if the concentration of dispersed phase is assumed to be dilute, inter-dispersed fluid collisions are negligible and the random motion of the dispersed phase is dominated by the turbulence in the continuous phase. Fluctuating quantities of the dispersed phase can, therefore, be given in terms of the mean characteristics of the continuous phase and the ratio of the dispersed fluid relaxation time and eddy-dispersed fluid interaction time.

A Reynolds Stress Model may be more appropriate for flows with sudden changes in strain rate or rotating flows.

2. 4. Effect of Turbulent Dispersion

Turbulent Dispersion Force results in additional dispersion of phases from high volume fraction regions to low volume fraction regions due to turbulent fluctuations. This is caused by the combined action of turbulent eddies and inter-phase drag. For example, in a dispersed two-phase flow, dispersed particles get caught up in continuous phase turbulent eddy, and are transported by the effect of inter-phase drag. The effect is to move particles from areas of high to low concentration. Hence, this effect will usually be important in turbulent flows with significant inter-phase drag.

In the context of dispersed liquid-liquid systems, the importance of turbulent dispersion has been recognized by quite a few investigators (Domgin *et al.*[23]; Soleimani *et al.*[40]; Hamad *et al.*[25]). As all models work towards homogenizing the dispersed phase distribution depending on the intensity of turbulence, the effect of turbulent dispersion has been demonstrated using just two models (Lopez and Favre)[41].

In this study two models for simulating inter-phase turbulent dispersion force were used:

2. 4. 1. Favre Averaged Drag Model

It is a model based on the Favre average of the inter-phase drag force:

$$F_{\mathrm{TD,p}} = F_{\mathrm{TD,q}} = -C_{\mathrm{TD}} C_{\mathrm{pq}} \frac{\upsilon_{\mathrm{tq}}}{\sigma_{\mathrm{tq}}} \left(\frac{\nabla \alpha_{\mathrm{p}}}{\alpha_{\mathrm{p}}} - \frac{\nabla \alpha_{\mathrm{q}}}{\alpha_{\mathrm{q}}} \right) \quad (18)$$

This model has been shown to have a wide range of universality. σ_{tc} is the turbulent Schmidt number for continuous phase volume fraction.

2. 4. 2. Lopez de Bertodano Model

The model of Lopez de Bertodano[34] was one of the first models for the turbulent dispersion force:

$$F_{\mathrm{TD,p}} = -F_{\mathrm{TD,q}} = -C_{\mathrm{TD}} \rho_{\mathrm{q}} k \nabla \alpha_{\mathrm{q}} \quad (19)$$

There is not a universally valid value of the non-dimensional Turbulent Dispersion Coefficient. Values of 0.1-0.5 have been used successfully for bubbly flow with bubble diameters of order of a few millimeters.

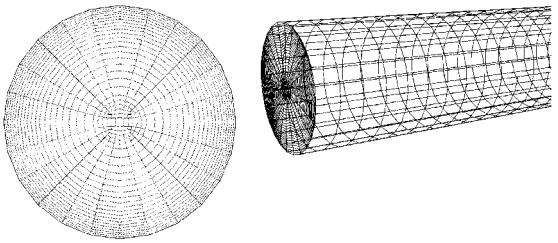

Fig. 1 A Typical Radial Grid Layout for a Geometry; 58,880 Cells (60,701 nodes)

3. Numerical Computation

3. 1. Numerical Method

To solve governing equations, the finite-volume scheme based on the FLUENT[42] code was employed and the SIMPLE method was applied for the pressure-velocity coupling. Moreover, second-order central difference was used for convective terms as inherent ability of second order schemes to suppress any non-physical 'wiggles,' in the CFD solution. As liquid-liquid vertical pipe flows feature steady state behavior, therefore, steady state conditions were assumed. A double-precision solver was employed in place of a single precision solver as disparate length scales were encountered in simulations. A three-dimensional model is used for all simulations. The standard k-ε model was used to account for turbulence.

Velocity inlet boundary condition was applied to define the flow velocity, along with all relevant scalar properties of the flow. A constant, uniform velocity, normal to the inlet boundary was specified in all the simulations. A pressure outlet boundary condition was used at the pipe exit. In the present study, a zero gauge pressure was specified at the outlet. Along the walls, no-slip boundary conditions were adopted.

A typical grid layout is shown in **Fig. 1**. As the geometry being modeled (cylindrical pipe) was quite simple, a structured hexahedral grid was used. The grid independence study was carried out using two grid resolutions. The grid sizes used for the independence system in simulating experiments were 58,880 and 120,000.

3. 2. Experimental Details

Farrar and Bruun[21] carried out experiments in a 1.5 m long pipe of 78 mm internal diameter with kerosene-water system. Hot film anemometry (HFA) was used for measuring the profile of holdup and velocity. Similar work was done by Al-Deen and Bruun[22] in a 1.5 m long pipe of 77.8 mm internal diameter (D). The distance between the entrance and the axial testing position was 16D (1.25 m) of straight vertical pipe. Summary of liquid-liquid data points and their experimental flow conditions are organized in **Table 2**.

Table 2 Summary of Experimental Flow Conditions for Selected Data Points

Data set	Data point	Pipe length and diameter		Continuous phase superficial velocity [m/s]	Dispersed phase superficial velocity [m/s]	Average experimental dispersed phase holdup [—]	Equivalent drop diameter [mm]	Total volumetric flow rate $(Q_p + Q_q)$ [m^3/s]
		L [m]	ID [mm]					
Farrar and Bruun[21]	F20	1.50	78	0.4935	0.1363	0.1912	5.00	0.00308
Al-Deen and Bruun[22]	A05	1.50	77.8	0.5441	0.0286	0.0493	3.00	0.00272

4. Results and Discussion

For accurate prediction of local hydrodynamics, it is extremely important to properly select the simulation parameters of the interfacial forces like lift force, drag force, dispersion force and virtual mass force. These selections should always be made based on the considerations of actual physics. For example, a proper choice of drag law and dispersed fluid (bubble/droplet) diameter is needed to accurately predict the slip velocity. So, it becomes important that one understands the interrelation between drag forces, dispersed fluid size and slip velocity. An attempt has been made here to elucidate this point.

The slip velocity, which can be considered as the signature of the multiphase system under a given condition, is given as:

$$V_s = \sqrt{\frac{4d_p}{3C_D}\left(\frac{\rho_q - \rho_p}{\rho_p}\right)g} \qquad (20)$$

From Eq. (20), it is clearly seen that, for a given value of drag force, slip velocity changes with bubble/droplet size. To understand this interrelation between drag forces, dispersed fluid size and slip velocity, slip velocity has been plotted as a function of dispersed fluid size for different drag laws (**Fig. 2**).

The list of drag laws considered and its expressions have been given in **Table 3**. From **Fig. 3**, it can be seen that a single value of slip can be obtained from several combinations of drag law and dispersed fluid size. Similarly, for a particular dispersed fluid size, one can obtain several values of slip depending on the drag law. It is, therefore, of prime importance to choose the correct combination of drag law and dispersed fluid size to model the gas-liquid flow in a dispersed fluid column or the liquid-liquid flow in a vertical pipe. Furthermore, with changes in superficial dispersed phase velocity, and the change in nature of two phase systems, the average dispersed fluid diameter changes, and hence, the value of slip velocity also changes.

Therefore, for different superficial velocities, either one has to take different dispersed fluid sizes, if drag law is constant; or select different drag laws, while keeping the dispersed fluid size constant. The first option is more realistic and represents the actual physical picture. Hence, it is always advisable to change the dispersed fluid size with change in superficial velocity. This elucidates the issue of proper choice of combination of drag law and dispersed fluid size as far as CFD simulation of vertical pipe hydrodynamics is concerned. Now, the drag force alone will not be sufficient to predict the local hydrodynamics correctly.

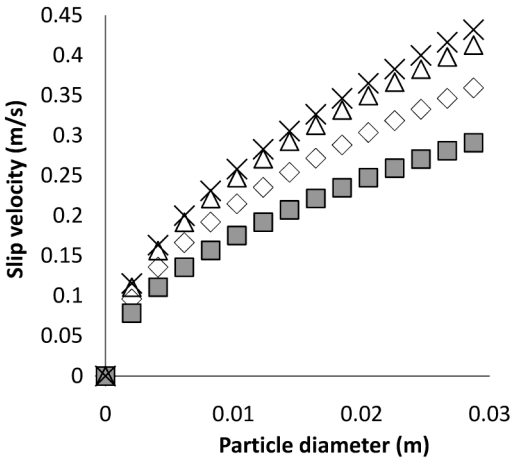

Drag models	CFD (present work)
$C_D = 0.44$	×
Schiller and Naumann[43]	△
Grace *et al.*[44]	◇
Ishii and Zuber[30]	■

Fig. 2 Comparison of Various Drag Models at Axial Position of 1.25 m

Table 3 Drag Laws Considered

Author	Model
Schiller and Naumann[43]	$C_D = \frac{24}{Re_p}\left(1 + 0.15 Re_p^{0.687}\right)$, if $Re_p = 1000$ $C_D = 0.44$, if $Re_p = 1000$
Grace *et al.*[44]	$C_D = \frac{4}{3}\frac{gd_p}{v_q^2}\frac{(r_q - r_p)}{r_q}$
Ishii and Zuber[30]	$C_D = \frac{2}{3}E_0^{0.5}$

Proper description of other interface forces such as lift force and dispersion force, are also important.

Therefore, to understand the effect of different interphase forces, a series of simulations have been carried out. For this purpose, the experimental data reported by Farrar and Bruun[21] have been considered.

4. 1. Effect of Drag Law

Simulations with all the drag laws given in **Table 3** have been carried out. The dispersed fluid sizes for all simulations have been chosen in such away to satisfy the average dispersed phase holdup. The various lift coefficients for the corresponding dispersed fluid size has been taken into account. Standard parameter settings are given in **Table 4**.

It can be seen from **Fig. 3** that though all the drag relations have been able to predict the average dispersed phase holdup and the centerline velocity quite accurately, the drag law reported by Ishii and Zuber[30] is closer to the experimental values.

4. 2. Effect of Lift Force

To study the effect of lift force, various values of C_L were chosen for the case given in **Table 4**. Simulations have been carried out with the value of $C_L = 0$ and the corresponding positive and negative values ($C_L = 0.005$, 0.001, 0.01, 0.1 and $C_L = -0.01$, -0.005, -0.003, -0.002), while other parameter values were same as that reported in **Table 4**. The results for holdup profile have been given in **Figs. 4a**, **4b**, **4c** and **4d**.

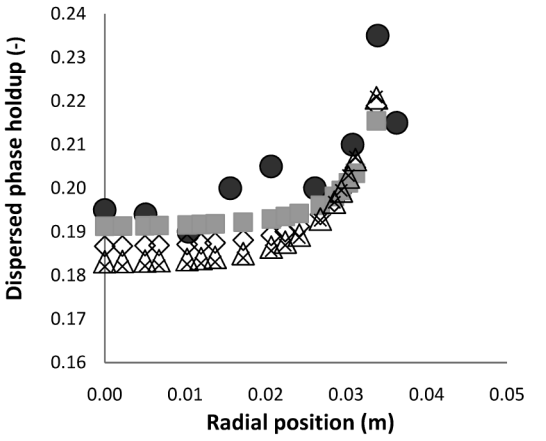

Drag models	CFD (present work)	Exp. F20
$C_D = 0.44$	×	
Schiller and Naumann[42]	△	●
Grace *et al.*[43]	◇	
Ishii and Zuber[30]	■	

Fig. 3 Effect of Various Drag Models on the Dispersed Phase Holdup at Axial Position of 1.25 m for the Data Set of Farrar and Bruun[21]

While positive value of C_L tends to predict increasing wall peaks, negative constants shift the dispersed phase holdup profiles towards an increased coring tendency. Referring to **Fig. 4a**, it can be seen that apart from the asymmetric nature of the holdup profiles when positive and negative constants of the same magnitude are used, the use of lift coefficients (*i.e.* $+0.01$ and -0.01) results in very low and high dispersed phase holdups at the wall. The flat holdup distribution for $C_L = 0$ corresponds to the case when only drag forces are accounted for.

However, lift force with a negative coefficient has to be used for the case of the dispersed fluid in order to capture the trends observed in experiments. It can be seen from **Fig. 4b** that the lift force can best be predicted using a negative coefficient ($C_L = -0.003$). **Figure 4c** shows the effect of positive lift coefficient on low dispersed phase holdup for the data set of Al-Deen and Bruun[22]. As expected, positive value of lift coefficients are closer to experimental data than negative values shown at **Fig. 4d**. As illustrated in **Fig. 4c** the closest value for lower holdup is $C_L = 0.01$.

4. 3. Effect of Turbulent Dispersion

Simulations were carried out with four values of C_{TD} based on Lopez de Bertodano's constant (0, 0.2, 0.5 and 1), and all the other parameters were kept the same as reported in **Table 4**.

Figure 5 shows that at low phase holdup although, C_{TD} value of 0.9 based on Favre average drag force was found to give a better agreement, but we feel the choice of the value C_{TD} is intuitive, depending on the system under consideration, which can predict the holdup and axial liquid velocity profile closer to the experimental value.

It can be seen from **Figs. 6a** and **6b** that at high phase fraction, the effect of C_{TD} differs with the sign of lift coefficient; however, it gives a completely different prediction near the wall when positive or negative lift coefficient is used. As a result, the effect of dispersion at higher holdups is not that significant, but at lower holdups, increase in value of C_{TD} makes the holdup pro-

Table 4 Standard Parameters Setting for Simulation (Farrar and Bruun[21] and Al-Deen[22])

		Farrar and Bruun (1996)	Al-Deen (1997)
Velocity [exp.]	[m/s]	0.6169	0.5727
Dispersed fluid diameter	[mm]	5	3
Lift force coefficient		-0.003	0.01
Turbulent dispersion force coefficient		0	0.9
Added mass force coefficient		—	—

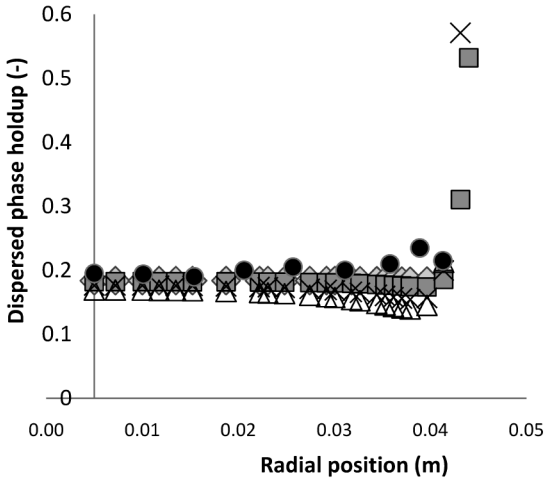

C_L	CFD (present work)	Exp. F20
0	◆	
0.001	■	
0.005	×	●
0.01	△	

Fig. 4a Effect of Positive Lift Coefficient on Dispersed Phase Holdup at Axial Position of 1.25 m for the Data Set of Farrar and Bruun[21)]

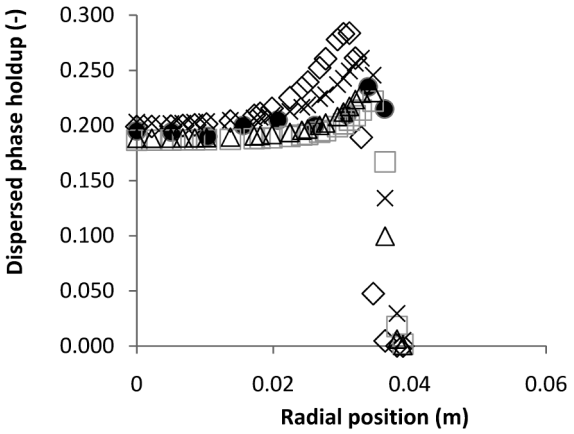

C_L	CFD (present work)	Exp. F20
− 0.01	◇	
− 0.002	□	
− 0.003	△	●
− 0.005	×	

Fig. 4b Effect of Negative Lift Coefficient on Dispersed Phase Holdup at Axial Position of 1.25 m for the Data Set of Farrar and Bruun[21)]

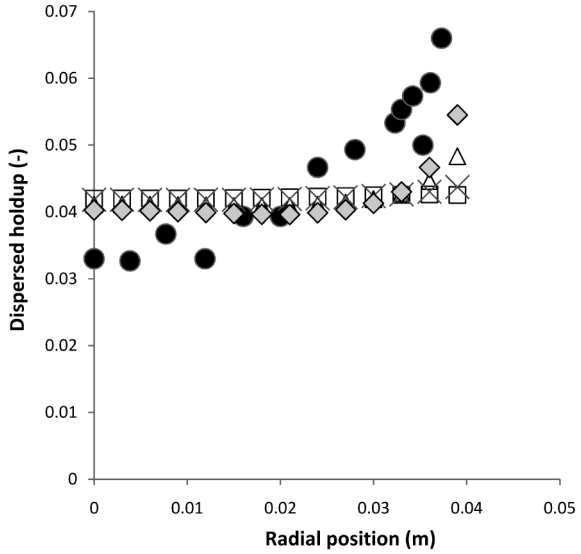

C_L	CFD (present work)	Exp. A05
0	□	
0.001	△	
0.005	×	●
0.01	◆	

Fig. 4c Effect of Positive Lift Coefficient on Low Dispersed Phase Holdup for the Data Set of Al-Deen and Bruun[22)] (Favre 0.9 for C_{TD}, lift constant varies and axial testing position is 1.25 m)

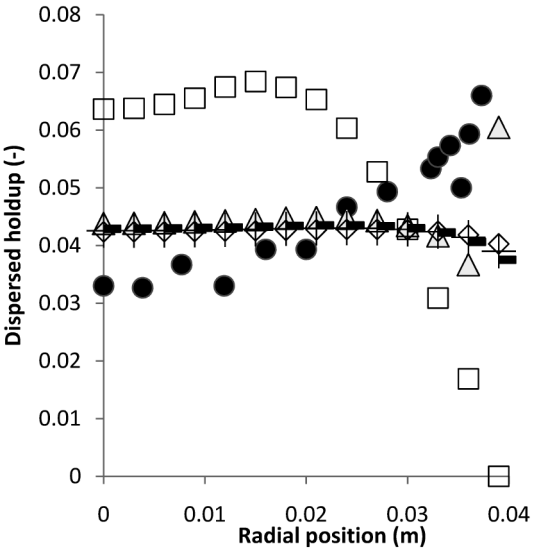

C_L	CFD (present work)	Exp. A05
− 0.1	□	
− 0.01	▲	
− 0.002	◇	●
− 0.003	+	
− 0.005	−	

Fig. 4d Effect of Negative Lift Coefficient on Low Dispersed Phase Holdup for the Data Set of Al-Deen and Bruun[22)] (Favre 0.9 for C_{TD}, lift constant varies and axial testing position is 1.25 m)

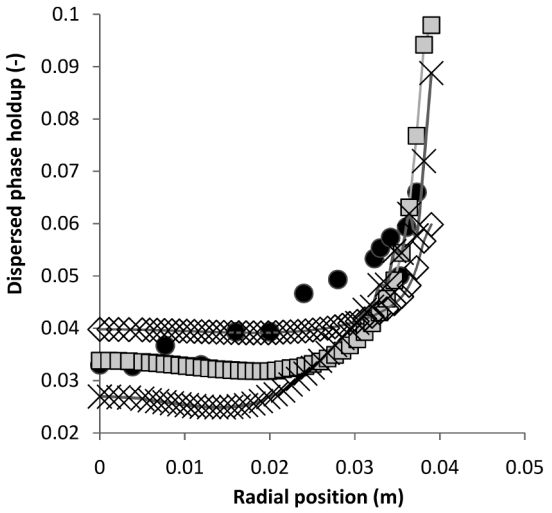

C_L	Favre	CFD (present work)	Exp. A05
0.01	0.7	◇	
0.04	0.9	■	●
0.09	0.9	×	

Fig. 5 Simulated Phase Distribution Profiles for the Data Set of Al-Deen and Bruun[22] (Favre for C_{TD}, lift constant varies and axial testing position is 1.25 m)

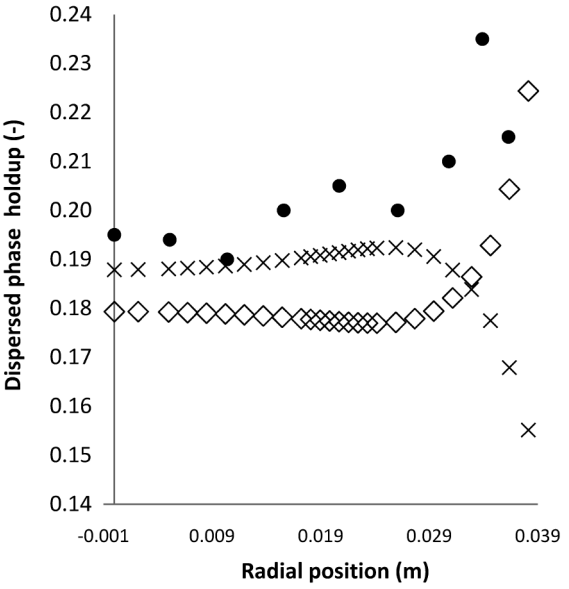

C_L	Lopez	CFD (present work)	Exp. F20
−0.003	0.1	×	●
0.003	0.1	◇	

Fig. 6a Simulated Phase Distribution Profiles for the Data Set of Farrar and Bruun[21] (Lopez 0.1, lift constant varies and axial position of 1.25 m)

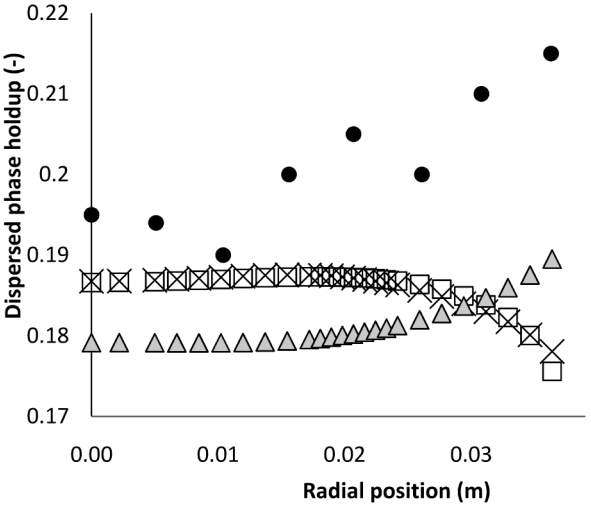

C_L	Lopez	CFD (present work)	Exp. F20
−0.003	0.5	×	
0	0.5	□	●
0.003	0.5	▲	

Fig. 6b Simulated Phase Distribution Profiles for the Data Set of Farrar and Bruun[21] (Lopez 0.5, lift constant varies and axial position of 1.25 m)

file comparatively flatter.

4. 4. Effect of Added or Virtual Mass Force

In fundamental nature, the virtual mass force is the force required to accelerate mass of the continuous phase in the immediate vicinity of the dispersed phase. It has the effect of dampening the natural tendency of the particle to accelerate in any direction. This force can be important near dispersed phase inlets and outlets and plays a particularly significant role when the density of the dispersed phase is much smaller than that of the continuous phase. It therefore is important in the case of bubbles and has no important effect on kerosene-water system (there are not much difference between densities of these two liquids). To observe the consequence of virtual mass, three simulations were carried out with $C_{VM} = 0$, 0.5 and 0.7. The results are given in **Fig. 7**. True to the previous prediction, it can be seen that, the addition of added mass force has no significant effect on results.

4. 5. Effect of Various Droplet Diameter

Most of the studies are focused on accounting for uniform size of droplets. As exact size distribution and even exact mean diameter for dispersed phase were not prescribed by any of investigators in their experiments, the equivalent drop diameter had to be guessed. Since previously mentioned in Eq. (20), some important parameters such as slip velocity and Reynolds number differ with diameter of drops. As shown in **Figs. 8** and **9**, the dispersed phase and continuous velocity profile vary with equivalent diameter at different radial positions. Then error of simulations for small drops can be neglected, but for accurate simulations, drop size distribution should be predicted and validated. Then

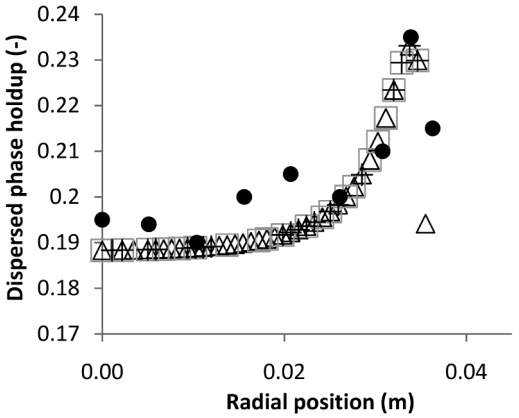

C_{VM}	CFD (present work)	Exp. F20
0	□	
0.5	△	●
0.7	+	

Fig. 7 Effect of Virtual Mass Coefficient on Dispersed Phase Holdup at Axial Position of 1.25 m for the Data Set of Farrar and Bruun[21] (Ishii and Zuber[30] expression for drag coefficient and −0.003 for lift coefficient)

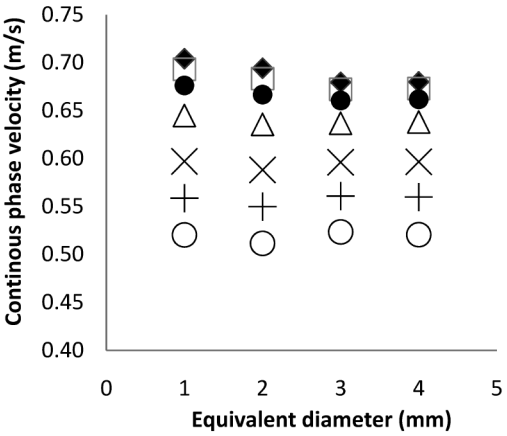

Radial positions [m]	CFD (present work)
0	◆
0.009	□
0.015	●
0.021	△
0.027	×
0.03	+
0.033	○

Fig. 8 Effect of Varying of Drop Diameter on the Holdup at Different Radial Positions and Axial Position of 1.25 m (Ishii and Zuber[30] expression for drag coefficient and −0.003 for lift coefficient)

simulation can be done accounting for size distribution of droplets. In these cases the use of methods such as population balance method is recommended.

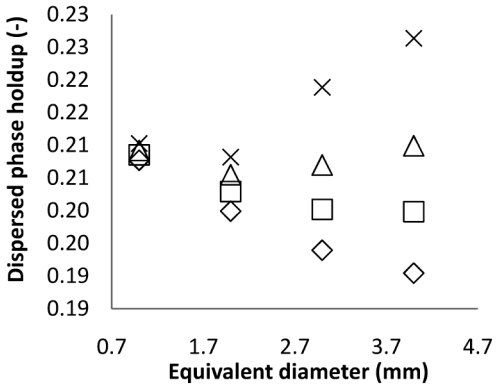

Radial positions [m]	CFD (present work)
0	◇
0.027	□
0.03	△
0.033	×

Fig. 9 Effect of Varying of Drop Diameter on the Continuous Phase Velocity at Different Radial Positions and Axial Position of 1.25 m (Ishii and Zuber[30] expression for drag coefficient and −0.003 for lift coefficient)

4. 6. Effect of Turbulence Model

The choice of a turbulence model depends on considerations such as the physics involved in the flow, the level of accuracy desired and the available computational resources. In the context of turbulent flows, the two-equation standard k-ε turbulence model is the most extensively studied and is, therefore, used as a baseline approach in RANS-based models. With specific reference to immiscible liquid dispersions, irrespective of the domain geometry, it is seen that the two-equation standard k-ε turbulence model is the most successful (reasonable accuracy, numerically robust and computationally economical) and, therefore, extensively used.

In this paper turbulence was modeled using standard k-ε turbulence model. An alternative approach (Reynolds Stress Model or RSM) was also tested. **Figures 10** and **11** show the comparison for radial profile of dispersed phase across the pipe for two different turbulence models at the experimental conditions of Farrar and Bruun[21] and Al-Deen and Bruun[22]. The RSM did not show better predictive performance than k-ε in predicting the average dispersed phase holdup. It is clear that the best turbulent model to apply at this case for all simulations is k-ε.

5. Conclusions

(1) For small equivalent drop diameter (≤3 mm), all available drag expressions for entities predict essentially similar holdups. On the other hand, significantly lower dispersed phase holdups were predicted when the drag expression for a rigid sphere was used in conjunction

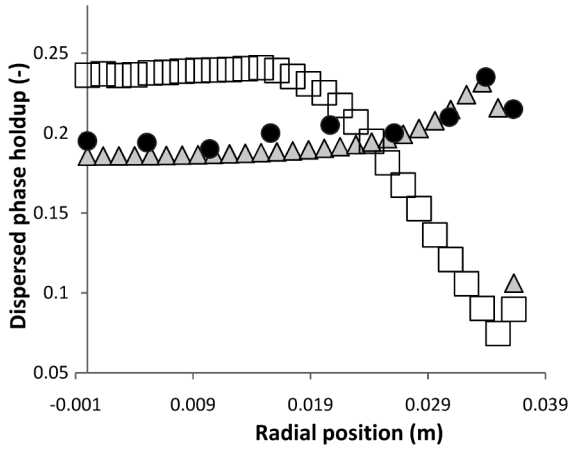

Fig. 10 Effect of Various Turbulent Models on the Dispersed Phase Holdup at Axial Position of 1.25 m for the Data Set of Farrar and Bruun[21] (Ishii and Zuber[30] expression for drag coefficient and −0.003 for lift coefficient)

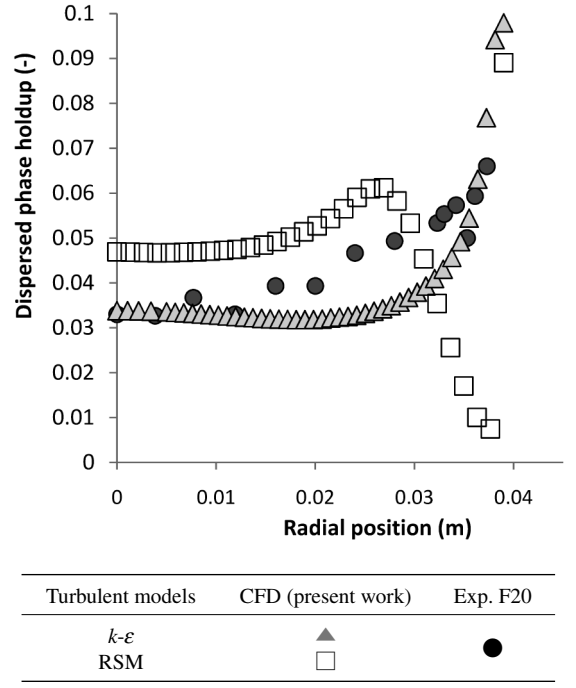

Fig. 11 Effect of Various Turbulent Models on the Dispersed Phase Holdup at Axial Position of 1.25 m for the Data Set of Al-Deen and Bruun[22] (Ishii and Zuber[30] expression for drag coefficient and −0.003 for lift coefficient)

with equivalent diameters larger than 5 mm. These are encountered at higher dispersed phase holdups where the increased coalescence tendency shifts the drop size distribution towards larger drops.

(2) The various drag expressions for drops predict essentially similar holdups. The drag expression proposed by Ishii and Zuber[30] was selected as a representative of the all drop drag expressions.

(3) Lift forces were found to play a significant role at both low and high dispersed phase holdups and their use is necessary to predict the experimentally observed wall peaking and coring profile. Lift force with a negative coefficient has to be used for the case of the bubbles in order to capture the trends observed in experiments. Then the lift forces can best be predicted using a negative coefficient −0.003 for high phase fractions and a positive coefficient 0.01 for low phase fractions.

(4) Dispersion forces act to spread out the dispersed phase in the solution domain thus counteracting lift forces. Turbulent dispersion was found to be significant at low dispersed phase holdups but is practically negligible at dispersed phase ratio larger than 25%. Similar conclusions apply for the dispersion model proposed by Lopez de Bertodano[32].

(5) At lower holdup range (≤5%) positive lift coefficient with a turbulent dispersion constant C_{TD} of 0.9 base on Favre[41] yields a better match with the data whereas in the case of higher holdups a constant lift coefficient of −0.003 without the turbulent dispersion produces a good agreement with the experimental data.

(6) No significant contribution of virtual mass force on the simulation of dispersed phase holdup in vertical pipe flow was seen.

(7) The performance of two turbulence models (standard k-ε and RSM) were compared with the experimental data of Farrar and Bruun[21] and Al-Deen and Bruun[22]. The RSM did not show better predictive performance than k-ε in predicting the average dispersed phase holdup.

Acknowledgment

We would like to acknowledge the fellowship help given by Srinath Madhavan.

Nomenclatures

C	: momentum transfer coefficient	[—]
C_D	: drag force coefficient	[—]
C_L	: lift force coefficient	[—]
C_m	: constant in k-ε model	[—]
C_S	: Smagorinsky constant	[—]
C_{TD}	: turbulent dispersion coefficient	[—]
C_{VM}	: virtual mass force coefficient	[—]
d	: drop diameter	[m]
E_0	: Eotvos number	[—]
F	: interface force	[N]
g	: gravitational constant	[m/s^2]
G	: generation term	[kg/m·s^2]
k	: turbulent kinetic energy per unit mass	[m^2/s^2]
$\dot{m}$	: mass flow rate	[kg/s]
P	: pressure	[N/m^2]
P'	: exact production term	[kg/m·s^3]
Re	: Reynolds number	[—]
S	: source term	[—]
t	: time	[s]

v	: velocity vector	[m/s]
v_s	: slip velocity	[m/s]
<Greeks>		
α	: fractional phase holdup	[—]
μ	: shear viscosity	[Pa·s]
ρ	: density	[kg/m^3]
$\overline{\rho v_i' v_j'}$	: Reynolds stresses	[N/m^2]
σ	: Prandtl number for turbulent kinetic energy	[—]
τ	: shear stress	[Pa]
λ	: bulk viscosity	[Pa·s]
φ	: turbulent kinetic energy	[m^2/s^3]
Φ	: pressure-strain correlation	[kg/m·s^3]
<Subscripts>		
p	: dispersed phase	
q	: continuous phase	
t	: turbulent	
<Superscript>		
—	: mean component	
’	: fluctuating component	
→	: vector quantity	

References

1) Friberg, P. C., Ph. D. Thesis, Dalhousie University, Canada, 1998.
2) Thakre, S. S., Joshi, J. B., *Chem. Eng. Sci.*, **54**, 5055 (1999).
3) Joshi, J. B., *Chem. Eng. Sci.*, **56**, 5893 (2001).
4) Sokolichin, A., Eigenberger, G., *AIChE J.*, **50**, 24 (2004).
5) Deen, N. G., Solberg, T., Hjertager, B. H., *Chem. Eng. Sci.*, **56**, 6341 (2001).
6) Dhotre, M. T., Joshi, J. B., *Trans. Inst. Chem. Eng.*, **78**, 689 (2004).
7) Jin, N., Wang, W., Liu, X., Tian, S., SPE International Oil and Gas Conference and Exhibition, Beijing, China, 7-10 Nov., 2000.
8) Brauner, N., “Modelling and Control of Two-Phase Phenomena: liquid-liquid two-phase flow systems,” Technical Report, 1-59 (2002).
9) Shi, M., Jepson, W. P., Rhyne, L. D., The SPE Annual Technical Conference and Exhibition, Denver, Colorado, USA., 5-8 Oct., 2003.
10) Madhavan, S., M. Sc. Thesis, Dalhousie University, Nova Scotia, Canada, 2005.
11) Jakobsen, H. A., SannZs, B. H., Grevskott, S., Svendsen, H. F., *Ind. Eng. Chem. Res.*, **36**, (10), 4052 (1997).
12) Ranade, V. V., Tayalia, Y., *Chem. Eng. Sci.*, **56**, (4), 1667 (2001).
13) Worner, M., “A Compact Introduction to the Numerical Modeling of Multiphase Flows,” Technical Report, 1-47 (2003).
14) Chen, P., Dudukovic, M. P., Sanyal, J., *AIChE J.*, **51**, 696 (2005).
15) Tabib, M. V., Roy, S. A., Joshi, J. B., *Chem. Eng. J.*, (2007), doi: 10.1016/j.cej.2007.09.015.
16) Rieger, R., *Comput. Chem. Eng.*, **18**, S229 (1994).
17) Modes, G., Bart, H. J., *Chem. Eng. Technol.*, **24**, 1242 (2001).
18) Vikhansky, A., Kraft, M., *Chem. Eng. Sci.*, **59**, 2597 (2004).
19) Alopaeus, V., Koskinen, J., Majander, J., *Chem. Eng. Sci.*, **57**, 1815 (2002).
20) Agterof, W. G. M., Vaessen, G. E. J., Haagh, G. A. A. V., Klahn, J. K., Jassen, J. M., *Colloids Surf.*, **31**, 141 (2008).
21) Farrar, B., Bruun, H. H., *Int. J. Multiphase Flow*, **22**, 733 (1996).
22) Al-Deen, M. F. N., Bruun, H. H., *Meas. Sci. and Technol.*, **8**, 885 (1997).
23) Domgin, J., Huilier, D. G. F., Burnage, H., Gardin, P., *J. Hyd. Res.*, **35**, 473 (1997).
24) Calabrese, R. V., Middleman, S., *AIChE J.*, **25**, 1025 (1979).
25) Hamad, F. A., Khan, M. K., Bruun, H. H., *Phonics J. Com. Flu. Dyn. and Its App.*, **12**, 19 (1999).
26) Farrar, Ph. D. Thesis, Bradford University, 1988.
27) Sabot, J., Ph. D. Thesis, Lyon University, 1976.
28) Lance, M., Lopez de Bertodano, M., *Mul. Sci. Tech.*, **8**, 69 (1994).
29) Bertodano, M. L., Lahey, R. T., Jones, O. C., *Int. J. Multiphase Flow*, **20**, 805 (1994).
30) Ishii, M., Zuber, N., *AIChE J.*, **25**, 843 (1979).
31) Wachem, B. G. M., Almstedt, A. E., *Chem. Eng. J.*, **96**, 81 (2003).
32) Drew, D. A., Lahey Jr, R. T., *Int. J. Multiphase Flow*, **13**, 113 (1987).
33) Hunt, J. C. R., Auton, T. R., Sene, K., Thomas, N. H., Kowe, R., ICHMT International seminar on transient phenomena in multiphase flow, Dubrovnik, Yugoslavia, 1987, p. 103-125.
34) Lopez de Bertodano, M., Ph. D. Thesis, Rensselaer Polytechnic Institute, Troy New York, 1991.
35) Lahey Jr., R. T., Lopez de Bertodano, M., Jones, O. C., *Nuclear Engineering and Design*, **141**, 177 (1993).
36) Peirano, E., Leckner, B., *Proc. Energy Combustion Sci.*, **24**, 259 (1998).
37) Balzer, G., Boelle, A., Simonin, O., Fludization VIII, Int. Symp. of the Engineering Foundation, Tours, 1995, p. 1125.
38) Simonin, O., “IMVU,” Meserburg, Germany (1995).
39) Enwald, H., Peirano, E., Almstedt, A. E., *Int. J. Multiphase Flow*, **22**, 21 (1996).
40) Soleimani, A., Lawrence, C. J., Hewitt, G. F., SPE Annual Technical Conference and Exhabition, Houston, Texas, 1999, p. 3-6.
41) Ansys CFX—Solver theory guide, 2006.
42) Fluent, “Fluent 6.1.22 user’s guide” (online). Available: www. fluentusers. com/fluent61/doc/ori/html/ug/main_pre. htm.
43) Schiller, L. A., Naumann, Z., *Ver Deutsch. Ing.*, **77**, 138 (1935).
44) Grace, J. R., Wairegi, T., Nguyen, T. H., *Trans. Inst. Chem. Eng.*, **54**, 167 (1976).

……

要　　旨

垂直管内流における油分散系の数値シミュレーション

Mahdi Parvini, Bahram Dabir, and Seyed Abolfazl Mohtashami

Dept. of Chemical Engineering, Amirkabir University of Technology, Hafez St., P.O. Box 15875/4413 Tehran, IRAN

非混合液体分散系を取り扱ったシステムは石油化学業界で広く用いられている。そして，石油化学の分野では界面熱・物質移動率は系全体の現象に強く影響を与えることが知られており，相間界面接触面積に依存している。本研究は垂直管における非混合液体分散系の数値流体解析（CFD）を行ったものである。二流体分散系に関しては二流体モデル（オイラー-オイラーモデル）が多相モデリング用に広く使用されており，特に適切な計算量で広範囲なホールドアップの詳細予測が必要な場合に使用される。連続相に水，分散相にケロセンを使用したCFDシミュレーション結果，Farrar と Bruun の実験結果，ならびにAl-Deen と Bruun の実験結果との比較を行った。これらのシミュレーションは乱流液体分散系において作用する抗力，揚力，乱流分散力，付加質量力等のさまざまな力の影響を確認するためにも行われた。最適なパラメーターの組合せを選定するため，これらの流体に作用する力を示すいくつかのモデルを使用したシミュレーションを行った。さらに，二つの異なる乱流モデルを使用したシミュレーションも行った。本研究の成果として，揚力が乱流分散力や付加質量力よりも重要であることが分かった。また，実験データと合致するシミュレーション結果をもとに，液液分散流における相間界面モデル化の指針を示すことができた。

……